BENDING-WAVE DIFFRACTION FROM STRIPS AND CRACKS ON THIN PLATES

By A. N. NORRIS and Z. WANG

(Department of Mechanical and Aerospace Engineering, Rutgers University, Piscataway, New Jersey 08855-0909, USA)

[Received 11 May 1993. Revise 27 January 1994]

SUMMARY

Two canonical problems concerning scattering of bending waves in thin plates are solved. The scatterers are either a semi-infinite rigid strip or a semi-infinite crack in an otherwise uniform plate of infinite extent. The exact scattered waves are represented by Fourier integrals obtained using the Wiener-Hopf method. The far-field diffraction coefficient for the rigid strip is independent of the material parameters, and is thus a universal parameter. The crack diffraction coefficient depends upon Poisson's ratio but this dependence is weak. Guided waves are generated on the free edges of the crack, and can be defined in terms of a separate diffraction coefficient which vanishes if Poisson's ratio is zero.

1. Introduction

When a wave strikes the tip of a crack in an elastic body it results in a diffraction pattern emanating from the tip as an equivalent source. The diffraction and scattering phenomenon is well understood for cracks in extended elastic bodies; see (1) for a review. However, there do not appear to be analogous solutions available for cracks in thin plates. Our purpose here is to fill this gap, and provide solutions for bending-wave diffraction from the tip of a crack in a thin plate. We also consider the dual problem of diffraction from the tip of a rigid strip in a thin plate.

We cast these problems within the framework of classical isotropic thin-plate theory for bending (2), and the solutions are found using the Wiener-Hopf method (3). The rigid strip is considered first because it is analytically easier. although the method of solution is essentially the same as for the crack. The crack is a 'mathematical' one in that its faces are infinitesimally close together but do not come in contact with one another. The solutions obtained here are of practical use within the limitations of thin-plate theory, which requires that the flexural wavelength be many (20 or more) times the thickness. Thin-plate singularities occur at the vertex or tip and these are not necessarily faithful representations of the stress-concentration mechanisms in real plates, which may have significant variations through the thickness. Despite the inaccuracy of the tip stresses we expect that the solution obtained here should be reasonable for estimating the scattered response from the tip. Further refinements to the present theory could be made, such as including rotary inertia and shear effects in the spirit of Mindlin's theory. One of the major points of our analysis is its relative simplicity, and it is offered as a first approximation to the full problem.

One novel aspect of the crack scattering problem is that we need to include the possibility of edge waves generated on the crack faces. This is similar to the presence of Rayleigh surface waves on the faces of a crack in bulk material (1), although the mechanics of the two waves are quite distinct. The edge mode for flexural waves, first noted by McKenna et al. (4) and discussed by Thurston and McKenna (5), is subsonic but very close in speed to the bulk flexural wave; in fact it reduces to a flexural wave with no decay away from the edge in the particular case of zero Poisson's ratio.

2. General theory

We consider an infinite thin plate with either a rigid strip or crack located on the half-line $0 \le x < \infty$, y = 0; see Fig. 1. The motion is time harmonic with the term $e^{-i\omega t}$ omitted but implicit throughout the paper. The transverse displacement of the plate is W(x, y) (complex-valued) and satisfies

$$\Delta^2 W - k^4 W = 0, (2.1)$$

where Δ is the two-dimensional Laplacian, and $k^4 = \omega^2 m/D$, with m the areal plate density and D the bending stiffness. The symbol W denotes the scattered field, and the total field is $W^{\text{total}} = W + W^{\text{inc}}$, where the incident field, W^{inc} , is of course also a solution to the bending-wave equation (2.1). We shall also need the bending moment M_v and the generalized Kirchhoff shear force V_v (2),

$$M_{y} = -D(vW_{,xx} + W_{,yy}), V_{y} = -D[(2 - v)W_{,xxy} + W_{,yyy}],$$
 (2.2)

where v is Poisson's ratio and the suffices preceded by a comma denote partial derivatives.

The analysis is simplified by treating the symmetric and antisymmetric problems separately. Split W as $W^S + W^A$, where $W^S(x, -y) = W^S(x, y)$ and

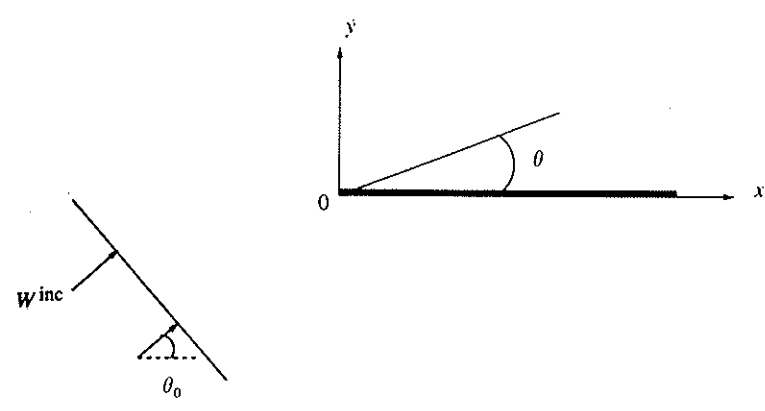


Fig. 1. The coordinate systems and the incident wave. The strip or crack occupies the half-line $x \ge 0$, y = 0

TABLE 1. The three conditions, (a), (b) and (c), for the four sub-problems considered

Condition and range	Rigid/	Rigid/	Crack/	Crack/
	Sym	Asym	Sym	Asym
(a) $f(x, 0) = 0, -\infty < x < \infty$	W,	W	V _y	M_{ν} W V_{ν}
(b) $f(x, 0) = 0, -\infty < x \le 0$	V,	M _y	W _y	
(c) $f(x, 0) = -f^{inc}(x, 0), 0 < x < \infty$	W	W _{.y}	M _y	

 $W^{\rm A}(x,-y)=-W^{\rm A}(x,y)$. Similarly, the incident field $W^{\rm inc}$ can be split; for example the symmetric part is $\frac{1}{2}[W^{\rm inc}(x,y)+W^{\rm inc}(x,-y)]$. There are four sub-problems, for the symmetric and antisymmetric scattering from the rigid strip and the crack. We deal with each one in turn. Superscripts S and A will be omitted where unnecessary, and we reiterate that the field W is the scattered response which satisfies radiation conditions. The total response is the sum of the incident and scattered fields. In each of the four sub-problems we have three conditions on y=0: (a), (b), and (c), which are determined by the symmetry and the boundary conditions on the scatterer. The conditions are defined on $-\infty < x < \infty$, $-\infty < x \le 0$, and $0 \le x < \infty$, respectively Table 1 lists the conditions for each sub-problem.

We need only consider the displacement in the half-space $y \ge 0$, with the remaining field determined by the prevailing symmetry. The scattered response is represented as

$$W(x, y) = \int_{-\infty}^{\infty} \left[A(\xi) e^{-\lambda k y} + B(\xi) e^{-\gamma k y} \right] e^{i\xi k x} \frac{d\xi}{2\pi}, \tag{2.3}$$

where

$$\lambda = (\xi^2 - 1)^{\frac{1}{2}}, \quad \gamma = (\xi^2 + 1)^{\frac{1}{2}}.$$
 (2.4)

We also define for later use the functions L and G, which enter into the expressions for the bending moment and shear force,

$$L(\xi) = (1 - \nu)\xi^2 - 1, \qquad G(\xi) = (1 - \nu)\xi^2 + 1.$$
 (2.5)

The radiation condition requires that the branch cuts of the square roots are chosen such that $\text{Re}(\gamma, \lambda) \ge 0$ and $\text{Im}(\gamma, \lambda) \le 0$ for $-\infty < \xi < \infty$. These ensure that the scattered field propagates away from the scatterer.

Unique solutions are obtained once we specify the conditions at the tip, which govern the nature of the mechanical singularity as $r \to 0$, where $r = (x^2 + y^2)^{\frac{1}{2}}$. In particular, we require that the thin-plate strain-energy density be integrable in the neighbourhood of the tip. The strain-energy density per unit area is a quadratic form in the second derivatives of W(x, y) (2). The behaviour of W near the origin depends upon the asymptotic dependence of the transform in

(2.3). Thus, if

$$A + B = O(\xi^{-\alpha}), \qquad |\xi| \to \infty, \tag{2.6}$$

then it is easily shown that

$$W = O(r^{(\alpha - 1)}), \qquad r \to 0, \tag{2.7}$$

and the second derivatives are of order $r^{(\alpha-3)}$. Hence, the strain energy is integrable if $2(\alpha-3) \ge -1$, or

$$\alpha \geqslant 5/2. \tag{2.8}$$

We shall show that the solutions are consistent with this tip condition.

3. Scattering from a rigid strip

3.1 The symmetric case

This is perhaps the simplest of the four cases, but it typifies the analysis for all of them. Conditions (a), (b) and (c), combined with the representation of (2.3) and (2.4), imply respectively, that

$$\lambda A(\xi) + \gamma B(\xi) = 0,$$

$$\lambda GA(\xi) + \gamma LB(\xi) = 2V^{-}(\xi),$$

$$A(\xi) + B(\xi) = W^{+}(\xi) + W^{-}(\xi),$$
(3.1)

where

$$W^{-}(\xi) = -\int_{0}^{\infty} W^{\text{inc}}(x,0) e^{-i\xi kx} k \, dx.$$
 (3.2)

The (a) equation is obvious; (b) comes from the fact that $V_{\nu}(x,0)$ vanishes for negative x and hence it can be represented by a transform like (2.3) with a function proportional to V^- , which must be analytic in the half-plane Im $\xi < 0$. The choice of the factor 2 is for later convenience. The functions W^+ and W^- in (c) are analytic in the upper and lower halves of the ξ -plane, respectively. The important point is that W^- is known from the boundary condition (c) in Table 1. The functions V^- and W^+ are unknown at this stage; their determination is the essence of the Wiener-Hopf problem. Eliminating A and B from (3.1) gives

$$\frac{V^{-}(\xi)}{K_{RS}(\xi)} = W^{+}(\xi) + W^{-}(\xi). \tag{3.3}$$

where

$$K_{\rm RS}(\xi) = \left(\frac{1}{\lambda} - \frac{1}{\gamma}\right)^{-1} = \frac{1}{2} \left[\gamma(\xi) + \lambda(\xi)\right] \gamma(\xi) \lambda(\xi). \tag{3.4}$$

The suffix R stands for 'rigid', and the S for 'symmetric'. The analytic splitting of $K_{RS} = K_{RS}^+ K_{RS}^-$ can be performed by the standard technique, see the Appendix

for details. Thus, $K_{RS}^+(\xi)$ and $K_{RS}^-(\xi)$ are analytic in the upper and lower half-planes, respectively.

We now assume that the incident field is a plane wave, such that the only singularity of W^- is a simple pole in the upper half-plane at $\xi = \xi_0$. Then (3.3) can be rearranged:

$$\frac{V^{-}(\xi)}{K_{RS}^{-}(\xi)} - K_{RS}^{+}(\xi_0)W^{-}(\xi) = K_{RS}^{+}(\xi)W^{+}(\xi) + W^{-}(\xi)[K_{RS}^{+}(\xi) - K_{RS}^{+}(\xi_0)].$$
(3.5)

Either side of this equation is analytic in a separate half-plane and therefore both are the same entire function $f(\xi)$ (analytic in the entire complex plane). We assume for the present that $f \equiv 0$, and will show later that any other form, such as a polynomial in ξ , yields a solution that is inconsistent with the tip condition (2.8). Therefore,

$$V^{-}(\xi) = K_{RS}^{+}(\xi_0) K_{RS}^{-}(\xi) W^{-}(\xi), \tag{3.6}$$

and using (3.1) to find A and B, equation (2.3) becomes explicit:

$$W(x, y) = K_{RS}^{+}(\xi_0) \int_{-\infty}^{\infty} K_{RS}^{-}(\xi) W^{-}(\xi) \left(\frac{1}{\lambda} e^{-\lambda k y} - \frac{1}{\gamma} e^{-y k y} \right) e^{i \xi k x} \frac{d\xi}{2\pi}.$$
 (3.7)

3.2 The rigid strip: antisymmetric case

The three equations are now

$$A(\xi) + B(\xi) = 0,$$

$$LA(\xi) + GB(\xi) = 2M^{-}(\xi),$$

$$\lambda A(\xi) + \gamma B(\xi) = T^{+}(\xi) + T^{-}(\xi),$$
(3.8)

where

$$T^{-}(\xi) = \frac{1}{k} \int_{0}^{\infty} W_{,y}^{\text{inc}}(x,0) e^{-i\xi kx} k \, dx. \tag{3.9}$$

Elimination of A and B leads to the Wiener-Hopf equation

$$\frac{M^{-}(\xi)}{K_{RA}(\xi)} = T^{+}(\xi) + T^{-}(\xi), \tag{3.10}$$

where

$$K_{\rm RA}(\xi) = \frac{1}{2} \left[\gamma(\xi) + \lambda(\xi) \right]. \tag{3.11}$$

Splitting $K_{RA} = K_{RA}^+ K_{RA}^-$, and assuming that the incident wave is a plane wave, we have

$$\frac{M^{-}(\xi)}{K_{RA}^{-}(\xi)} - K_{RA}^{+}(\xi_0)T^{-}(\xi) = K_{RA}^{+}(\xi)T^{+}(\xi) + T^{-}(\xi)[K_{RA}^{+}(\xi) - K_{RA}^{+}(\xi_0)],$$

analogous to (3.5). By the same arguments, we have

$$M^{-}(\xi) = K_{RA}^{+}(\xi_0)K_{RA}^{-}(\xi)T^{-}(\xi), \tag{3.13}$$

and equation (2.3) becomes

$$W(x, y) = -K_{RA}^{+}(\xi_0) \int_{-\infty}^{\infty} K_{RA}^{-}(\xi) T^{-}(\xi) (e^{-\lambda k y} - e^{-\gamma k y}) e^{i\xi k x} \frac{d\xi}{2\pi}.$$
 (3.14)

3.3 The rigid strip: full solution

Let the incident field be a plane wave of unit amplitude with propagation direction making an angle θ_0 with the strip, and incident from $y = -\infty$; specifically,

 $W^{\text{inc}} = e^{ik(x\cos\theta_0 + y\sin\theta_0)}, \qquad 0 \le \theta_0 < \pi, \tag{3.15}$

This range of incident angles is sufficient. Thus, $\xi_0 = \cos \theta_0$, $W^- = i/(\xi - \xi_0)$, and $T^- = \lambda(\xi_0) W^-$. Combining equations (3.7) and (3.14) and using

$$K_{RS}(\xi) = \lambda(\xi)\gamma(\xi)K_{RA}(\xi)$$
(3.16)

gives the total scattered field as

$$W(x, y) = \frac{i}{2\pi} \int_{-\infty}^{\infty} K_{RA}^{+}(\xi_{0}) K_{RA}^{-}(\xi) \frac{e^{i\xi kx} d\xi}{\xi - \xi_{0}} \times \left[\frac{\lambda^{+}(\xi_{0})\gamma^{+}(\xi_{0})}{\lambda^{+}(\xi)\gamma^{+}(\xi)} (\gamma e^{-\lambda k|y|} - \lambda e^{-\gamma k|y|}) - \lambda(\xi_{0})(e^{-\lambda k|y|} - e^{-\gamma k|y|}) \operatorname{sgn} y \right],$$
(3.17)

where λ^+ , γ^+ , etc., are defined in the Appendix. This equation is valid for all x and y. The behaviour near the origin is easily surmised: the results in the Appendix imply that $K_{RA}^- = O(\xi^{\frac{1}{2}})$ as $|\xi| \to \infty$, and therefore, referring to equation (2.6), we have $\alpha = 5/2$. This is consistent with an integrable singularity at the tip, from (2.8). It can now be seen in retrospect that had we taken any entire function $f(\xi)$ other than zero the singularity would turn out to be non-integrable. For example, $f = \text{constant} \neq 0$ yields $\alpha = 3/2$, which does not satisfy (2.8).

Let the observation point be defined by $x = r \cos \theta$ and $y = r \sin \theta$, $0 \le \theta \le 2\pi$; see Fig. 1. The contribution from the pole at $\xi = \xi_0$ yields the specular contributions to the scattered field: the shadow and the reflection. The 'shadow' is defined in the forward region $\theta < \theta_0$, in which the pole gives a contribution of $W = -W^{\text{inc}}$, as expected. The reflection from the rigid strip occurs on the 'lit' side, and its contribution from the pole is

$$W(x, y) = -2K_{RA}(\xi_0) \left[K_{RA}(\xi_0) \exp\{\lambda(\xi_0) k y\} - \lambda(\xi_0) \exp\{\gamma(\xi_0) k y\} \right] e^{i\xi_0 k x}$$

$$= \left\{ R(\theta_0) \exp(-iky \sin \theta_0) - \left[1 + R(\theta_0) \right] \exp\{ky(1 + \cos^2 \theta_0)^{\frac{1}{2}} \right\}$$

$$\times \exp(ikx \cos \theta_0), \quad 2\pi - \theta_0 < \theta < 2\pi, \quad (3.18)$$

where the reflection coefficient R is

$$R(\theta) = -\cos^2 \theta + i \sin \theta (1 + \cos^2 \theta)^{\frac{1}{2}}$$
$$= -\exp\{-i \cos^{-1} \cos^2 \theta\}. \tag{3.19}$$

This agrees, as expected, with the case of reflection from an infinite rigid strip. Note that $|R(\theta)| = 1$ for real angles of incidence, as one might expect from energy-flux conservation, and the phase of R is a smooth function of θ .

In addition to these specular effects the far field depends upon the 'diffraction coefficient' $D(\theta_0, \theta)$, defined such that

$$W = D(\theta_0, \theta) \left(\frac{2}{\pi k r}\right)^{\frac{1}{2}} e^{-i\pi/4} e^{ikr}, \qquad r \to \infty, \ 0 < \theta \leqslant 2\pi.$$
 (3.20)

This contains the far-field information about the flexural wave in regions where there is neither shadow nor reflection. We can also define D in the shadow and reflection zones, although it is singular on the shadow and reflection boundaries, $\theta = \theta_0$, and $\theta = 2\pi - \theta_0$, respectively. The singularity arises from the definition (3.20); one could develop a uniform solution valid across these boundaries using standard methods (1). The diffraction coefficient can be found from (3.17) by using the asymptotic integral approximation

$$\int_{-\infty}^{\infty} Q(\xi) \exp\left\{ikr(\xi\cos\theta + i\lambda(\xi)|\sin\theta|)\right\} d\xi \approx Q(\cos\theta)|\sin\theta| \left(\frac{2\pi}{kr}\right)^{\frac{1}{2}} e^{-i\pi/4} e^{ikr},$$

$$kr \to \infty. \quad (3.21)$$

We note that $\lambda(\xi) = -i(1-\xi^2)^{\frac{1}{2}}$ for $-1 \le \xi \le 1$, and so the asymptotic result follows by the method of stationary phase, where the stationary phase point occurs at $\xi = \cos \theta$. Hence, equations (3.17), (3.20) and (3.21) imply that

$$D(\theta_0, \theta) = \frac{K_{RA}^+(\cos \theta_0) K_{RA}^-(\cos \theta)}{2(\cos \theta_0 - \cos \theta)}$$

$$\times \left[\sin \theta_0 \sin \theta + \lambda^+ (\cos \theta_0) \gamma^+ (\cos \theta_0) \lambda^- (\cos \theta) \gamma^- (\cos \theta) \right]. \quad (3.22)$$

We note from (A.3) and (A.15) in the Appendix that D satisfies the symmetries

$$D(\theta_0, \theta) = \begin{cases} D(\pi - \theta, \pi - \theta_0), & 0 < \theta \leq \pi, \\ D(\theta - \pi, 2\pi \cup \theta_0), & \pi < \theta \leq 2\pi, \end{cases}$$
where the basis of $\pi \neq 0$ is $\pi = 0$. (3.23)

as one would expect on the basis of reciprocity.

It is interesting to compare the diffracted field, which is directionally dependent, with the quasi-monopole scattering field from a point constrained to be fixed. Thus, if an infinite, homogeneous plate is fixed at r = 0, the scattered field is easily found to be

$$W(r,\theta) = -H_0^{(1)}(kr) + H_0^{(1)}(ikr), \qquad (3.24)$$

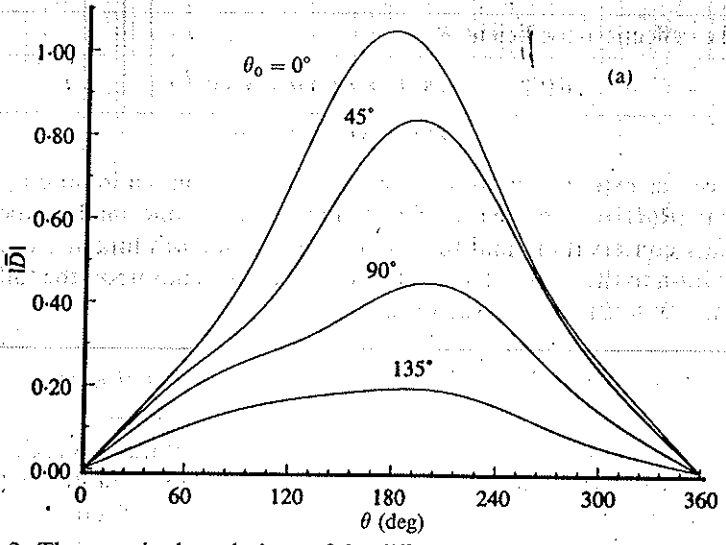


Fig. 2. The magnitude and phase of the diffraction coefficient for a rigid strip, from (3.22). The smooth quantity $\bar{D} \equiv D(\theta_0, \theta)(\cos \theta_0 - \cos \theta)/2$ is plotted to avoid the singularities in the specular directions. (a) shows the magnitude

where $H_0^{(1)}$ is the Hankel function of the first kind of order zero. It is easily seen that this solution has the desired property that $W(0, \theta) = -1$. In particular, the diffraction coefficient for the fixed point is -1. Plots of the amplitude and phase of the diffraction coefficient $D(\theta_0, \theta)$ of (3.22) are shown in Fig. 2. These curves consider the smooth parameter $D(\theta_0, \theta)(\cos \theta_0 - \cos \theta)/2$, which is of order unity in magnitude. One case of particular interest is for backscatter of a wave incident straight towards the strip, $\theta_0 = 0$, $\theta = \pi$, for which

$$D(0, \pi) = -\frac{1}{2}(1+i)K_{RA}^{+}(1)K_{RA}^{-}(-1)$$

$$= -0.9384 + i0.4743$$

$$= 1.0515 e^{i2.67379}.$$
(3.25)

This is only slightly larger in magnitude than the diffraction from a fixed point (unity), but the phase, $153\cdot19^\circ$, is appreciably different. The curves in Fig. 2 indicate that the diffracted bending-wave amplitude is generally largest in all directions for head-on incidence, $\theta_0 = 0$. Also, apart from the particular case discussed above for $\theta_0 = 0$, $\theta = \pi$, the diffracted amplitude is smaller than unity, and tends to zero in the direction of the strip.

4. Diffraction from a crack

4.1 The symmetric and antisymmetric solutions

Proceeding as before, the three equations for the symmetric problem are

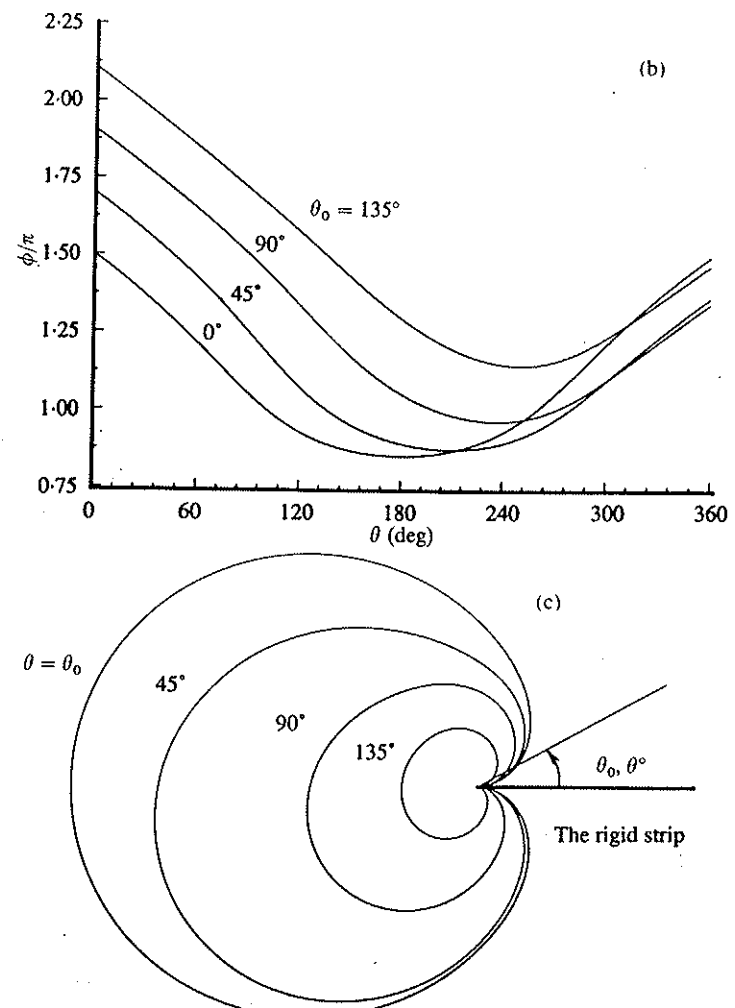


Fig. 2. (Continued) (b) the phase, defined by $\bar{D} = |D| \exp[i\phi]$, and (c) a polar plot of the magnitude for different angles of incidence

$$\lambda GA(\xi) + \gamma LB(\xi) = 0,
\lambda A(\xi) + \gamma B(\xi) = -2T^{-}(\xi),
LA(\xi) + GB(\xi) = M^{+}(\xi) + M^{-}(\xi),$$
(4.1)

where

$$M^{-}(\xi) = \frac{1}{Dk^2} \int_0^\infty M_y^{\text{inc}}(x,0) e^{-i\xi kx} k \, dx. \tag{4.2}$$

The Wiener-Hopf equation is

$$\frac{T^{-}(\xi)}{K_{CS}(\xi)} = M^{+}(\xi) + M^{-}(\xi), \tag{4.3}$$

where

$$K_{\rm CS}(\xi) = \left(\frac{L^2}{\lambda} - \frac{G^2}{\gamma}\right)^{-1}.\tag{4.4}$$

Solving as before, and using (2.3) and (4.1), the scattered field is found to be

$$W(x, y) = K_{CS}^{+}(\xi_0) \int_{-\infty}^{\infty} \frac{d\xi}{2\pi} K_{CS}^{-}(\xi) M^{-}(\xi) \left\{ \frac{L}{\lambda} e^{-\lambda k y} - \frac{G}{\gamma} e^{-\gamma k y} \right\} e^{i\xi k x}.$$
 (4.5)

Similarly, the antisymmetric equations for the crack become

$$LA(\xi) + GB(\xi) = 0,$$

$$A(\xi) + B(\xi) = -2W^{-}(\xi),$$

$$\lambda GA(\xi) + \gamma LB(\xi) = V^{+}(\xi) + V^{-}(\xi).$$
(4.6)

where

$$V^{-}(\xi) = \frac{1}{Dk^3} \int_0^\infty V_y^{\rm inc}(x,0) e^{-i\xi kx} k \, dx. \tag{4.7}$$

The Wiener-Hopf equation is now

$$\frac{W^{-}(\xi)}{K_{CA}(\xi)} = V^{+}(\xi) + V^{-}(\xi), \tag{4.8}$$

where

$$K_{\text{CA}}(\xi) = (\gamma L^2 - \lambda G^2)^{-1}.$$
 (4.9)

The antisymmetric scattered field reduces to

$$W(x, y) = -K_{CA}^{3}(\xi_{0}) \int_{-\infty}^{\infty} \frac{d\xi}{2\pi} K_{CA}^{-}(\xi) V^{-}(\xi) [G e^{-\lambda k y} - L e^{-\gamma k y}] e^{i\xi k x}. \quad (4.10)$$

Note that the functions for the symmetric and antisymmetric cases are related by

$$K_{\rm CS} = \lambda \gamma K_{\rm CA},\tag{4.11}$$

and hence the analytic splitting for both is very similar.

4.2 The full solution

We again consider excitation by the incident plane wave (3.15). Using the relations $(2.2)_1$ and $(2.2)_2$ we obtain

$$M^{-}(\xi) = \frac{iL(\xi_0)}{\xi - \xi_0}, \qquad V^{-}(\xi) = \frac{iG(\xi_0)\lambda(\xi_0)}{\xi - \xi_0}.$$
 (4.12)

Combining equations (4.5) and (4.10) and using (4.11) and (4.12), the total scattered field is found as

$$W(x, y) = \frac{i}{2\pi} \int_{-\infty}^{\infty} K_{CA}^{+}(\xi_{0}) K_{CA}^{-}(\xi) \frac{e^{i\xi kx} d\xi}{\xi - \xi_{0}}$$

$$\times \left[\frac{\lambda^{+}(\xi_{0}) \gamma^{+}(\xi_{0})}{\lambda^{+}(\xi) \gamma^{+}(\xi)} L(\xi_{0}) (L\gamma e^{-\lambda k|y|} - G\lambda e^{-\gamma k|y|}) - G(\xi_{0}) \lambda(\xi_{0}) \right]$$

$$\times (G e^{-\lambda k|y|} - L e^{-\gamma k|y|}) \operatorname{sgn} y . \tag{4.13}$$

This equation is valid for all x and y. The integral has been simplified so that it involves only the function K_{CA} and not K_{CS} . The analytic splitting of K_{CA} is discussed in detail in the Appendix, from which we see that $K_{CA}^- = O(\xi^{-\frac{1}{2}})$ as $|\xi| \to \infty$. The parameter α of equation (2.6) therefore follows as $\alpha = 5/2$, which implies that the solution has an integrable singularity at the tip. Had we assumed a non-zero entire function in the analytic splitting of the Wiener-Hopf equation (4.3) then the solution would have a non-integrable singularity at the tip, in violation of the thin-plate theory.

As before, we note that the pole at $\xi = \xi_0$ gives the shadow $W = -W^{\text{inc}}$ in the shadow region, and in the reflection zone we get

$$W(x, y) = \left\{ R(\theta_0) \exp(-iky \sin \theta_0) + \left[\frac{1 + R(\theta_0)}{1 - (1 - v)^2 \cos^4 \theta_0} \right] \right.$$

$$\times \exp\{ky(1 + \cos^2 \theta_0)^{\frac{1}{2}} \right\} \exp(ikx \cos \theta_0), \quad 2\pi - \theta_0 < \theta < 2\pi,$$
(4.14)

where R is now the reflection coefficient for a free edge,

$$R(\theta) = \frac{\lambda G^2 + \gamma L^2}{\lambda G^2 - \gamma L^2} \Big|_{\xi = \cos \theta}$$

$$= \frac{-(\sin^2 \theta + \nu \cos^2 \theta)^2 (1 + \cos^2 \theta)^{\frac{1}{2}} + i \sin \theta [1 + (1 - \nu) \cos^2 \theta]^2}{(\sin^2 \theta + \nu \cos^2 \theta)^2 (1 + \cos^2 \theta)^{\frac{1}{2}} + i \sin \theta [1 + (1 - \nu) \cos^2 \theta]^2}.$$
(4.15)

It is clear that |R| = 1 for any angle, and the phase of R is plotted in Fig. 3. The value at $\theta = \frac{1}{2}\pi$ agrees with the reflection coefficient for a flexural wave at a free end of a beam, R = i. However, unlike the reflection coefficient for the rigid boundary conditions, the phase of R is not necessarily a smooth function of θ . We shall say more about this and its consequences below.

A crack-tip diffraction coefficient may be defined in the same manner as for the rigid strip, using equation (3.20). Following the same type of analysis we

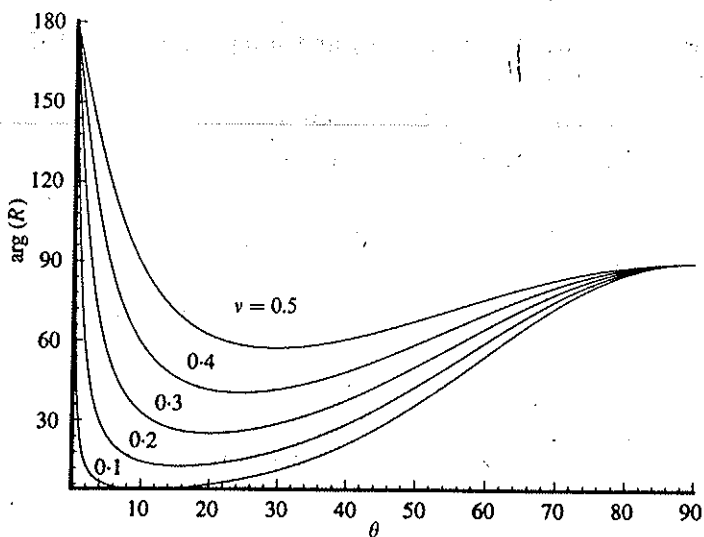


Fig. 3. The phase of the reflection coefficient, $R(\theta)$, for plane-wave reflection from a free edge, from (4.15). The phase is defined by $R(\theta) = \exp[i\phi]$, and is plotted in degrees

find that

$$D(\theta_0, \theta) = \frac{K_{CA}^+(\cos \theta_0) K_{CA}^-(\cos \theta)}{2(\cos \theta_0 - \cos \theta)} \left[\sin \theta_0 G(\cos \theta_0) \sin \theta G(\cos \theta) + \lambda^+(\cos \theta_0) \right] \times \gamma^+(\cos \theta_0) L(\cos \theta_0) \lambda^-(\cos \theta) \gamma^-(\cos \theta) \times L(\cos \theta)$$

$$\times L(\cos \theta) \left[(4.16) \right]$$

It is clear that this diffraction coefficient also satisfies the reciprocity relations of (3.23). Figure 4 shows plots of the diffraction coefficient for various angles of incidence. Note that the diffracted field is generally smallest for head-on incidence, $\theta_0 = 0$. It is also interesting to compare the curves in Fig. 4 with the analogous curves for the rigid strip in Fig. 2. The overall dependence of the diffracted amplitude on the angle of incidence in one case is roughly the reverse of that in the other. The dependence upon Poisson's ratio is illustrated in Fig. 5.

4.3 The diffracted edge waves

Both K_{CS} and K_{CA} possess four simple poles at the same points, $\xi = \pm \beta$, $\pm i\beta$, which are the roots of $E(\xi) = 0$, where the edge function E is

$$E(\xi) = L^2 \gamma - G^2 \lambda, \tag{4.17}$$

and β is the positive root of

$$\beta^4 = \frac{1 - 3\nu + 2(1 - 2\nu + 2\nu^2)^{\frac{1}{2}}}{(3 + \nu)(1 - \nu)^2}.$$
 (4.18)

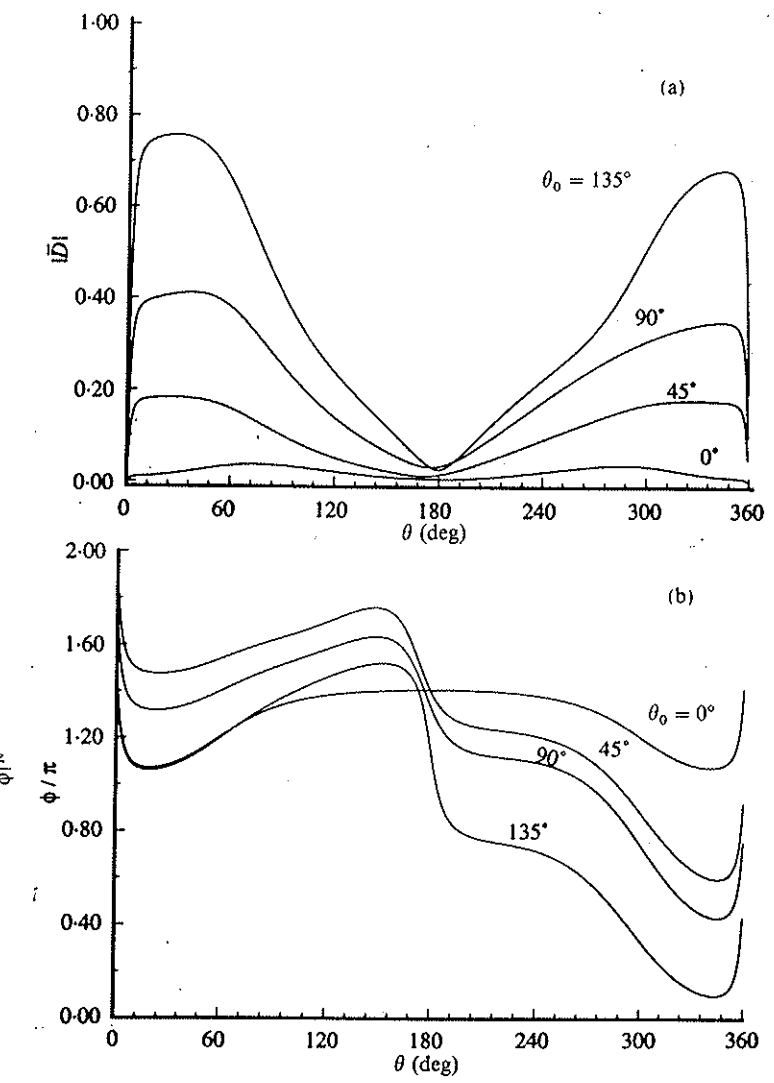


Fig. 4. The diffraction coefficient for the crack. The quantity $\bar{D} \equiv D(\theta_0, \theta)$ (cos $\theta_0 - \cos \theta$)/2, with D given by (4.16), is plotted to avoid the specular singularities. (a) magnitude, (b) phase

Thurston and McKenna (5) first showed that $\xi = \beta$ is a root, which may be seen by multiplying $E(\xi)$ by $L^2\gamma + G^2\lambda$, and then solving the resulting quadratic equation for ξ^4 . At the same time, it can be easily checked that the three other roots of (4.18) are also roots of E = 0: the negative root $\xi = -\beta$ follows because $E(\xi)$ is an even function for real ξ , and the imaginary roots are an immediate consequence of the property $E(i\xi) = iE(\xi)$, also for real valued ξ . It can be easily

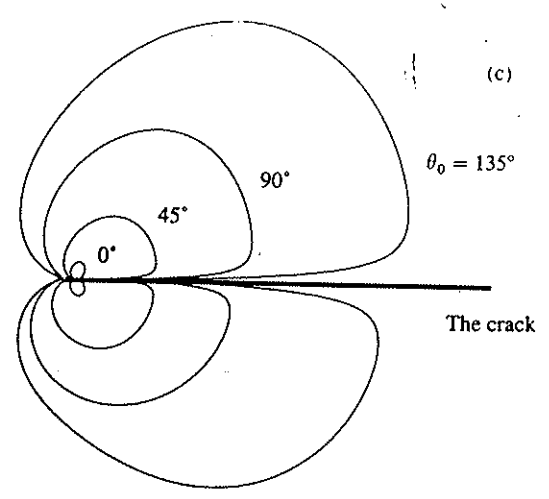


Fig. 4. (Continued) (c) polar plot of the magnitude, all for v = 0.3

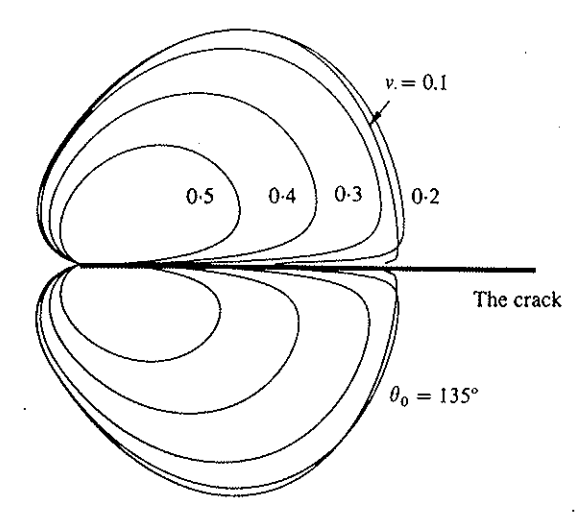


Fig. 5. Polar plots of the magnitude of $\widetilde{D} \equiv D(\theta_0,\theta)(\cos\theta_0-\cos\theta)/2$ for $\theta_0=135^\circ$ and for different values of Poisson's ratio

verified, by applying the principle of the argument (6) to the function E, that there are only four roots to E=0.

It is clear, by rewriting (4.18) in the form

$$\frac{1}{\beta^4} = 1 - \left[\left((1 - \nu)^2 + \nu^2 \right)^{\frac{1}{2}} - (1 - \nu) \right]^2 \tag{4.19}$$

that $\beta \ge 1$ with equality only if $\nu = 0$. The existence of the poles $\xi = \pm \beta$ at 'subsonic' speed is associated with the possibility of guided edge waves along

the free edge of a plate, first noted by McKenna et al. (4) and discussed in detail by Thurston and McKenna (5). These authors noted that the free edge relieves the transverse stresses associated with flexural waves, and so reduces the speed relative to the flexural wave. This effect vanishes for v = 0, in which case the surface wave becomes a plane wave travelling parallel to the boundary. It turns out that although $\beta > 1$, the difference $\beta - 1$ is very small, which follows from the expansion of (4.18),

$$\beta = 1 + v^4 (1 + 2v + \frac{5}{2}v^2 + 2v^3 + \cdots)/16. \tag{4.20}$$

Thus, the surface wave is very slowly decaying away from the boundary, and is essentially like a plane wave travelling along the boundary. The poles at the imaginary values $\xi = \pm i\beta$ imply that evanescent edge waves are also possible.

The scattered field of (4.13) generates edge waves on the two faces of the crack, x > 0, $y = \pm 0$. The amplitudes of these waves follow from the general expression (4.13) by noting that $K_{CA}(\xi)$ has a simple pole at $\xi = \beta$. The amplitude of the edge wave on the faces of the crack may be written as

$$W(x, \pm 0) = D_{\pm}^{\text{edgc}}(\theta_0) e^{i\beta kx}, \quad \text{edge wave,}$$
 (4.21)

where the edge-wave diffraction coefficient is determined by evaluating the residue of the integrand in (4.13) at $\xi = \beta$. Using the result (A.26) we find that

$$D_{\pm}^{\text{edge}}(\theta_{0}) = \frac{2\beta K(\beta) K_{\text{CA}}^{+}(\beta)}{\left[K^{+}(\beta)\right]^{2}} \frac{\gamma^{-}(\beta)}{\gamma^{+}(\beta)} \frac{K_{\text{CA}}^{+}(\cos\theta_{0})}{\beta - \cos\theta_{0}}$$

$$\times \left\{ i\lambda^{+}(\cos\theta_{0})\gamma^{+}(\cos\theta_{0})L(\cos\theta_{0}) \left[G(\beta)\frac{\lambda^{-}(\beta)}{\gamma^{+}(\beta)} - L(\beta)\frac{\gamma^{-}(\beta)}{\lambda^{+}(\beta)}\right] \right\}$$

$$\pm 2\sin\theta_{0}G(\cos\theta_{0}) \right\}, \tag{4.22}$$

where the quantity $K(\beta)$ is given in (A.25). Note that the \pm on D_{\pm}^{edge} refers to the upper (y = +0) or lower (y = -0) faces of the crack. Plots of the diffraction coefficient are given in Fig. 6.

The dependence of the edge-wave diffraction coefficient upon v as $v \to 0$ may be surmised from the results presented in the Appendix, particularly the asymptotic behaviour of $K(\beta)$ in (A.27). Apart from the special case of head-on incidence, for which θ_0 is near zero and is discussed in detail next, we find that

$$D_{+}^{\text{edge}}(\theta_0) = O(v^2), \qquad v \to 0,$$
 (4.23)

and hence no edge waves are generated in this limit. However, in the same limit the concept of the edge wave is ill-defined because the bulk wave propagating parallel to the crack faces satisfies the no-stress conditions there, but is not evanescent away from the edges. This wave is also defined by the bulk-wave diffraction coefficients $D(\theta_0^{\dagger}, 0)$ and $D(\theta_0, 2\pi)$ on the faces y = +0 and y = -0, respectively.

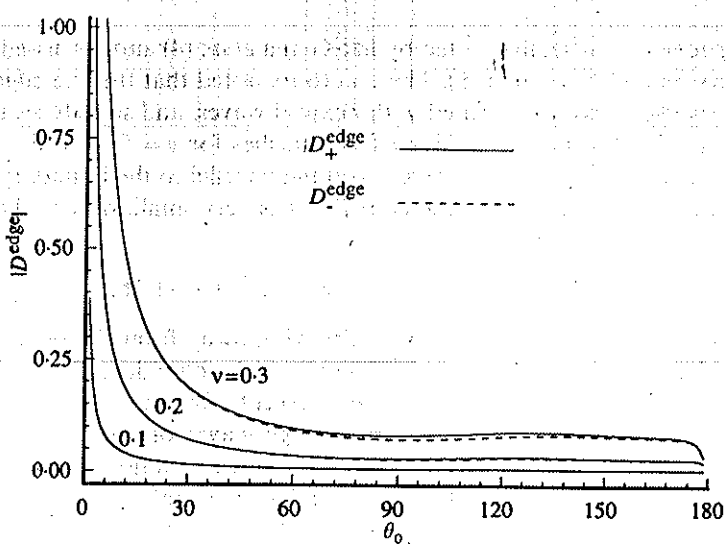


Fig. 6. The magnitude of the edge-wave diffraction coefficients, D_{+}^{edge} and D_{-}^{edge} of (4.22), for different values of v

Both the edge-wave amplitude from (4.21) and the reflection coefficient, $R(\theta_0)$ of (4.15), behave irregularly near the double point $\theta_0 = v = 0$. This is evident in the rapid variation in the phase of $R(\theta_0)$, shown in Fig. 3, as $\theta_0 \to 0$, particularly for small values of v. This phase sensitivity is associated with the pole nearby at $\xi = \beta$, and the sensitivity is stronger for smaller values of v because, as equation (4.20) indicates, the pole tends to unity monotonically from above as v tends to zero. Expanding the two coefficients for small v and θ_0 , with the specific scaling $\theta_0 = O(v^2)$, and using the expansions of equations (4.20) and (A.27) which hold in this limit, we find that

$$R \to -\left(\frac{v^2 - i\sqrt{8\theta_0}}{v^2 + i\sqrt{8\theta_0}}\right), \quad D_{\pm}^{\text{edge}} \to 2v^2 \left(\frac{v^2 \pm i\sqrt{8\theta_0}}{v^4 + 8\theta_0^2}\right), \quad v, \, \theta_0 \to 0. \quad (4.24)$$

Thus, R(0) = -1 for $v \neq 0$, but if we set v = 0 and then take the limit $\theta_0 \to 0$ we find R = +1, in agreement with the behaviour depicted in Fig. 3. Similarly, putting $\theta_0 = 0$ and then performing the limit of $v \to 0$ yields $D_{\pm}^{\text{edge}} \to 2$. On the other hand, setting v = 0 first, yields $D_{\pm}^{\text{edge}} = 0$. We note, however, that the limiting value of the sum $(R + D_{\pm}^{\text{edge}})$ is constant and equal to unity on the lower, or lit, face y = -0.

The cause of this apparently non-analytic state of affairs is that in the double limit of both $\theta_0 \to 0$ and $\nu \to 0$ the edge wave becomes indistinguishable from the reflected bulk wave. The description of the scattered field in terms of the individual parts, reflected plus edge wave plus diffraction, is not suitable, but rather, the edge wave and reflected bulk wave should be viewed together, particularly near the tip where their phases are virtually the same. More

generally, the phases along the crack edge of the two waves are βkx and kx, and therefore as long as the difference is small we should consider the waves as a single phenomenon. This will be the case for values of x such that $(\beta - 1)kx = o(1)$. In this region the phases are coherent.

We may calculate the combined effect in the coherent zone as follows. For simplicity, we assume that $\theta_0 = 0$, so that the effect is due to the merging of the poles at $\xi = \beta$ and $\xi = 1$. In the limits as $\beta \to 1$ the two simple poles becomes a double pole, and hence their residue contribution vanishes. Thus,

$$\frac{1}{(\xi - \xi_0)(\xi - \beta)} = \frac{1}{\beta - 1} \left(\frac{1}{\xi - \beta} - \frac{1}{\xi - \xi_0} \right) \to \frac{1}{(\xi - 1)^2}.$$
 (4.25)

The combined effect follows using (4.13) and (4.25), evaluating the pole contributions (branch-cut contribution may be ignored as being of smaller order), giving

$$W(x, \pm 0) = \nu K_{CA}^{+}(1) \left[\text{res } K_{CA}^{-}(\beta) \right] \left\{ \frac{f(\beta) - f(1)}{\beta - 1} \right\} e^{ikx}, \tag{4.26}$$

where the residue can be determined from (A.26), and

$$f(\xi) = \frac{\lambda^{+}(1)\gamma^{+}(1)}{\lambda^{+}(\xi)\gamma^{+}(\xi)}(L\gamma - G\lambda). \tag{4.27}$$

Expanding the right-hand member of (4.26) for small v implies that

$$W(x, \pm 0) = e^{ikx} \left[\sqrt{2\nu + O(\nu^2)} \right], \qquad \nu \to 0.$$
 (4.28)

Thus, the diffracted edge wave on either face resulting from head-on incidence $(\theta_0 = 0)$ disappears as Poisson's ratio vanishes. The general dependence of the edge-wave amplitude in equation (4.26) as a function of ν is shown in Fig. 7.

5. Conclusion

The same type of Wiener-Hopf analysis could be applied to flexural wave scattering from semi-infinite impedance strips, of which the rigid strip is a limiting case (infinite impedance). By generalizing the thin-plate constitutive theory one could also consider scattering from strips or cracks in orthotropic thin plates, where the scatterer is aligned with a principal direction. Edge waves are also possible in orthotropic thin plates (7), and so the analysis for the crack would again involve a function possessing poles at slightly subsonic wavenumbers.

Acknowledgment

This work was supported by the US Office of Naval Research, under the supervision of Dr Geoffrey Main.

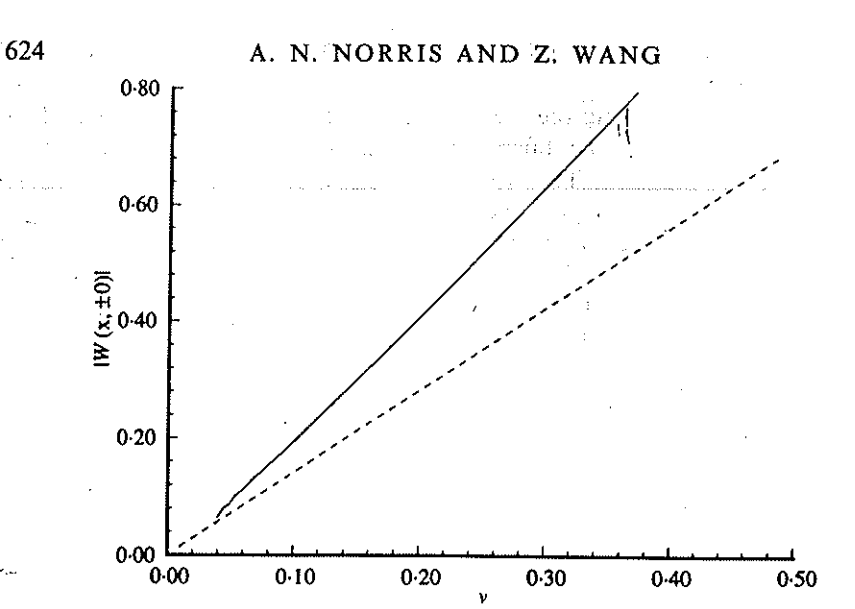


Fig. 7. The magnitude of the edge wave in the coherent zone for head-on incidence, $\theta_0 = 0$, from (4.26). The dashed curve in the straight line $W = \sqrt{2v}$

APPENDIX

Analytic factorization

The analytic factorization of the functions γ and λ of (2.4) is straightforward (3). We

$$\lambda^{\pm} = e^{-i\pi/4} (1 \pm \xi)^{\frac{1}{2}}, \quad \gamma^{\pm} = (1 \mp i\xi)^{\frac{1}{2}},$$
 (A.1)

so that

$$\lambda(\xi) = \lambda^{+}(\xi)\lambda^{-}(\xi), \qquad \gamma(\xi) = \gamma^{+}(\xi)\gamma^{-}(\xi). \tag{A.2}$$

The plus and minus functions are analytic in the upper and lower half-planes, respectively, and have the symmetry properties

$$\lambda^{+}(-\xi) = \lambda^{-}(\xi), \quad \gamma^{+}(-\xi) = \gamma^{-}(\xi), \quad \xi \text{ real.}$$
 (A.3)

Consider a function $F(\xi)$ which has the property that $F(\xi) \to 0$ as $|\xi| \to \infty$. We may then write F as a sum of functions analytic in either half-plane, $F(\xi) = F^+(\xi) +$ $F^{-}(\xi)$, where (3, 1)

$$F^{+}(\xi) = \frac{1}{2\pi i} \int_{-\infty + id}^{\infty + id} \frac{F(t)}{t - \xi} dt, \quad \text{Im } \xi \geqslant 0,$$

$$F^{-}(\xi) = \frac{-1}{2\pi i} \int_{-\infty + ic}^{\infty + ic} \frac{F(t)}{t - \xi} dt, \quad \text{Im } \xi \leqslant 0,$$
(A.4a)

$$F^{-}(\xi) = \frac{-1}{2\pi i} \int_{-\infty + i\epsilon}^{\infty + i\epsilon} \frac{F(t)}{t - \xi} dt, \quad \text{Im } \xi \leqslant 0,$$
 (A.4b)

and Im $\xi = d$, c delineate the lower and upper boundary of the common strip of analyticity, with d < 0 < c. The functions we are interested in factorizing are symmetric in ξ , $F(-\xi) = F(\xi)$, and therefore we have from (A.4) that

$$F^{+}(-\xi) = F^{-}(\xi), \quad \xi \text{ real.}$$
 (A.5)

We consider the rigid problem first, for which we let

$$F(\xi) = \ln \frac{1}{2} \left(1 + \frac{\lambda(\xi)}{\gamma(\xi)} \right), \tag{A.6}$$

so that

$$K_{\rm RA}(\xi) = \gamma(\xi) e^{F(\xi)},\tag{A.7}$$

and

$$K_{\mathrm{RA}}^{\pm}(\xi) = \gamma^{\pm}(\xi) e^{F \pm (\xi)}. \tag{A.8}$$

Also, consider $\xi \ge 0$. The integral for $F^+(\xi)$ can be deformed into the lower half-plane, where it meets the continuous branch cut along the union of the line strips $-1 \le t \le 0$ and $0 \le t \le -i$, which has the outline of an inverted letter L. The quantity $\lambda(\xi)$ is purely imaginary but discontinuous across the cut. On the northern and eastern faces $\lambda(\xi) = -i(1-\xi^2)^2$, whereas $\lambda(\xi) = i(1-\xi^2)^2$ on the other faces. And $\gamma(\xi) = (1+\xi^2)^2$ on all faces. Therefore, (A.4) becomes

$$F^{+}(\xi) = \frac{1}{2\pi i} \left\{ \int_{-1}^{0} + \int_{0}^{-t} g(t) \frac{dt}{t - \xi}, \right\}$$
(A.9)

where

$$g(t) = \ln \left[\frac{(1+t^2)^{\frac{1}{2}} - i(1-t^2)^{\frac{1}{2}}}{(1+t^2)^{\frac{1}{2}} + i(1-t^2)^{\frac{1}{2}}} \right] = -i2 \tan^{-1} \left(\frac{1-t^2}{1+t^2} \right)^{\frac{1}{2}}.$$
 (A.10)

It is observed that $\xi=0$ is a singular point for the above integral. To remove it we rewrite (A.9) as

$$F^{+}(\xi) = \frac{1}{2\pi i} \left\{ \int_{-1}^{0} + \int_{0}^{-i} \left\{ \left[g(t) - g(0) \right] \frac{dt}{t - \xi} + \frac{g(0)}{2\pi i} \left\{ \int_{-1}^{0} + \int_{0}^{-i} \left\{ \frac{dt}{t - \xi}, \right\} \right\} \right\}$$
(A.11)

The second integral of (A.11) has an explicit form

$$I(\xi) = \left\{ \int_{-1}^{0} + \int_{0}^{-i} \frac{dt}{t - \xi} = \ln \frac{(1 + \xi^{2})^{\frac{1}{2}}}{1 + \xi} + i \cot^{-1} \xi. \right.$$
 (A.12)

Noting that $g(0) = -\frac{1}{2}i\pi$, it follows from (A.9) to (A.12) that $\frac{1}{2}i\pi = \frac{1}{2}i\pi$, it follows from (A.9) to (A.12) that

$$F^{+}(\xi) = \frac{1}{\pi} \int_{0}^{1} \left[\frac{1}{s+\xi} + \frac{1}{s-i\xi} \right] \left[\tan^{-1} \left(\frac{1-s^{2}}{1+s^{2}} \right)^{\frac{1}{2}} - \frac{\pi}{4} \right] ds - \frac{1}{4} I(\xi). \tag{A.13}$$

The function $K_{RA}^+(\xi)$ may be computed from this relation and (A.8) by numerical integration. The form chosen in (A.13) is numerically efficient for $\xi \ge 0$ even as $\xi \to 0$ since the integrand remains bounded near s=0 in this limit. For ξ real but negative, we may use (A.5) to write $K_{RA}^+(\xi) = \gamma^+(\xi) \exp\{F(\xi) - F^+(-\xi)\}$. In summary, for ξ real,

$$K_{RA}^{+}(\xi) = \begin{cases} \gamma^{+}(\xi) \exp[F^{+}(\xi)], & \xi \ge 0, \\ \frac{K_{RA}(\xi)}{\gamma^{-}(\xi)} \exp[-F^{+}(-\xi)], & \xi < 0, \end{cases}$$
(A.14)

and the minus function is evaluated using the symmetry property

$$K_{RA}^{-}(\xi) = K_{RA}^{+}(-\xi), \quad \xi \text{ real.}$$
 (A.15)

These forms avoid the complication of evaluating principal-value integrals and are used in the numerical calculations.

The special case of $\xi = 0$ serves as a useful check on the integration code. Equation (A.5) implies that $F^+(0) = \frac{1}{2}F(0) = \frac{1}{2}\ln\left[\frac{1}{2}(1-i)\right]$. We can also verify this result directly from the integral for F^+ by noting that for $\xi = 0$ the integral in (A.13) reduces to

$$\int_0^1 \left[\frac{\pi}{4} - \tan^{-1} \left(\frac{1 - s^2}{1 + s^2} \right)^{\frac{1}{2}} \right] \frac{ds}{s} = \int_0^{\frac{1}{4}\pi} \left[\frac{\pi}{4} - \theta \right] \tan 2\theta \ d\theta = \frac{1}{8}\pi \ln 2, \tag{A.16}$$

where we have used the substitution $\tan \theta = ((1-s^2)/(1+s^2))^{\frac{1}{2}}$ and the result

$$\lim_{\theta \to \frac{1}{4}\pi} \left(\frac{1}{4}\pi - \theta \right) \ln(\cos 2\theta) = 0. \tag{A.17}$$

Hence, we obtain the identity $F^+(0) = -\frac{1}{4} \ln 2 - \frac{1}{8} i \pi$, in agreement with the previous value for the same quantity. Therefore, letting $\xi \to 0$, either formula in (A.14) gives the same answer, $K_{RA}^+(0) = 2^{-\frac{1}{4}} e^{-i\pi/8}$, which can be compared with the numerical result as a check.

In order to split the crack functions K_{CS} and K_{CA} , of (4.4) and (4.9), we consider the related function

$$K(\xi) = -(1 - \nu)(3 + \nu)(\xi^4 - \beta^4) K_{CA}(\xi) / \gamma(\xi)$$

$$= -(1 - \nu)(3 + \nu) \frac{(\xi^4 - \beta^4)}{\gamma(\xi) E(\xi)},$$
(A.18)

where $E(\xi)$ is defined in (4.17) and β is the surface wavenumber, from (4.18). The function $K(\xi)$ has no poles at the edge wavenumbers $\xi = \pm \beta$, $\pm i\beta$, and it tends to unity as $|\xi| \to \infty$. Hence we can use the same methods as above to first write

$$\ln K = F^{+} + F^{-}, \tag{A.19}$$

where F + has the same form as before, (A.9), but with

$$g(t) = -i2 \tan^{-1} \left[\frac{G^2(t)}{L^2(t)} \left(\frac{1 - t^2}{1 + t^2} \right)^{\frac{1}{2}} \right]. \tag{A.20}$$

Proceeding as before we find by analogy with (A.13) that

$$\ln K^{+}(\xi) = \frac{1}{\pi} \int_{0}^{1} \left[\frac{1}{s+\xi} + \frac{1}{s-i\xi} \right] \left\{ \tan^{-1} \left[\frac{G^{2}(s)}{L^{2}(s)} \left(\frac{1-s^{2}}{1+s^{2}} \right)^{\frac{1}{2}} \right] - \frac{\pi}{4} \right\} ds - \frac{1}{4} I(\xi). \tag{A.21}$$

where $I(\xi)$ is given by (A.12). The splitting of $K_{\rm CA}$ then follows from (A.18) as

$$K_{CA}^{+}(\xi) = \begin{cases} \frac{\gamma^{+}(\xi)K^{+}(\xi)}{(\beta + \xi)(\beta - i\xi)((1 - \nu)(3 + \nu))^{\frac{1}{2}}}, & \xi \ge 0, \\ K_{CA}(\xi)/K_{CA}^{+}(-\xi), & \xi < 0, \end{cases}$$
(A.22)

and

$$K_{CA}^{-}(\xi) = K_{CA}^{+}(-\xi), \quad \xi \text{ real.}$$
 (A.23)

These forms have the desirable property that they avoid the evaluation of principal-value

integrals and are used for numerical calculations. The case of $\xi = 0$, for which

$$K^{+}(0) = \sqrt{(K(0))} = \beta^{2} ((1 - \nu)(3 + \nu))^{\frac{1}{2}} 2^{-\frac{1}{4}} e^{-i\pi/8}, \tag{A.24}$$

again provides a check for the numerical code.

The residue of the functions K_{CA} , K_{CS} , K_{CA}^- , etc., at the pole $\xi = \beta$ can be easily determined from the value of K at $\xi = \beta$. The latter can be reduced to the following form, using equations (4.18) and (A.18):

$$K(\beta) = \frac{(1-\nu)^2(3+\nu)(\beta^2-1)\beta^2}{(1-2\nu+2\nu^2-(1-2\nu+2\nu^2)^{\frac{1}{2}})} \frac{G(\beta)}{L(\beta)}.$$
 (A.25)

In particular, we need the residue of K_{CA}^- , which can be expressed, using equations (A.18), (A.22), (A.23), and (A.25), as

res
$$K_{CA}^-|_{\xi=\beta} = i2\beta \frac{K_{CA}^+(\beta)K(\beta)}{[K^+(\beta)]^2} \frac{\gamma^-(\beta)}{\gamma^+(\beta)}$$
. (A.26)

The value of $K(\beta)$ increases monotonically from zero to 0.295799... as ν goes from zero to $\frac{1}{2}$, and near zero it has the Taylor—series expansion

$$K(\beta) = \frac{3}{4}v^2 + v^3 + \cdots$$
 (A.27)

Thus, the strength of the pole, and hence the edge wave, diminishes as $\nu \to 0$. Finally, we note that the function K simplifies in the special case of $\nu = 0$, for which $G = \gamma^2$ and $L = \lambda^2$, and

$$K(\xi) = \frac{3}{2} \left(\frac{\xi^2 - 1 + \lambda \gamma}{2\xi^2 + \lambda \gamma} \right), \qquad \nu = 0.$$
 (A.28)

In this case the poles disappear as they merge with the branch points at $\xi = \pm 1$ and $\xi = \pm i$.

REFERENCES

- J. D. ACHENBACH, A. K. GAUTESEN and H. McMaken, Ray Methods for Waves in Elastic Solids (Pitman, Boston 1982).
- 2. S. Timoshenko, Theory of Plates and Shells (McGraw-Hill, New York 1940).
- B. NOBLE, Methods Based on the Wiener-Hopf Technique for the Solution of Partial Differential Equations (Pergamon Press, New York 1958).
- J. MCKENNA, G. D. BOYD and R. N. THURSTON, IEEE Trans. Sonics Ultrasonics 21 (1974) 178-186.
- 5. R. N. THURSTON and J. McKenna, ibid. 21 (1974) 296-297.
- J. D. ACHENBACH, Wave Propagation in Elastic Solids (North-Holland, Amsterdam 1973).
- 7. A. N. Norris, J. Sound Vib. 171 (1994) 571-573.